Methanol immersion reduces spherical aberration of water dipping lenses at long wavelengths used in multi-photon laser scanning microscopy

Greg Norris,[*] **Ayman Gebril, Valerie A. Ferro, and Gail McConnell**

Centre for Biophotonics, Strathclyde Institute for Pharmaceutical and Biomedical Sciences, University of Strathclyde, 161 Cathedral Street, Glasgow, G4 0RE, UK

*greg.norris@strath.ac.uk

Abstract: Dipping objectives were tested for multi-photon laser scanning microscopy, since their large working distances are advantageous for thick specimens and the absence of a coverslip facilitates examination of living material. Images of fluorescent bead specimens, particularly at wavelengths greater than 850 nm showed defects consistent with spherical aberration. Substituting methanol for water as the immersion medium surrounding the beads corrected these defects and produced an increase in fluorescence signal intensity. The same immersion method was applied to two representative biological samples of fixed tissue: mouse brain labeled with FITC for tubulin and mouse gut in which the Peyer's patches were labeled with Texas Red bilosomes. Tissue morphology was well preserved by methanol immersion of both tissues; the two-photon-excited fluorescence signal was six times higher than in water and the depth of penetration of useful imaging was doubled. No modification of the microscope was needed except the provision of a ring to retain a sufficient depth of methanol for imaging.

References and links

1. W. Denk, J. H. Strickler, and W. W. Webb, "Two-photon laser scanning fluorescence microscopy," Science **248**(4951), 73–76 (1990).
2. F. Helmchen and W. Denk, "Deep tissue two-photon microscopy," Nat. Methods **2**(12), 932–940 (2005).
3. M. D. Cahalan, I. Parker, S. H. Wei, and M. J. Miller, "Two-photon tissue imaging: seeing the immune system in a fresh light," Nat. Rev. Immunol. **2**(11), 872–880 (2002).
4. P. Theer, M. T. Hasan, and W. Denk, "Two-photon imaging to a depth of 1000 μm in living brains by use of a Ti:Al$_2$O$_3$ regenerative amplifier," Opt. Lett. **28**(12), 1022–1024 (2003).
5. D. Débarre, W. Supatto, A. M. Pena, A. Fabre, T. Tordjmann, L. Combettes, M. C. Schanne-Klein, and E. Beaurepaire, "Imaging lipid bodies in cells and tissues using third-harmonic generation microscopy," Nat. Methods **3**(1), 47–53 (2006).
6. M. J. Booth and T. Wilson, "Refractive-index-mismatch induced aberrations in single-photon and two-photon microscopy and the use of aberration correction," J. Biomed. Opt. **6**(3), 266–272 (2001).
7. C. J. Sheppard and M. Gu, "Aberration compensation in confocal microscopy," Appl. Opt. **30**(25), 3563–3568 (1991).
8. F. P. Bolin, L. E. Preuss, R. C. Taylor, and R. J. Ference, "Refractive index of some mammalian tissues using a fiber optic cladding method," Appl. Opt. **28**(12), 2297–2303 (1989).
9. G. Norris, R. Amor, J. Dempster, W. B. Amos, and G. McConnell, "A promising new wavelength region for three-photon fluorescence microscopy of live cells," J. Microsc. **246**(3), 266–273 (2012).
10. W. Denk, D. W. Piston, and W. W. Webb, "Multi-photon molecular excitation in laser-scanning microscopy," in *Handbook of Biological Confocal Microscopy*, J. B. Pawlay, ed. (Springer Science, 2006), pp. 535–549.
11. F. J. Kao, M. K. Huang, Y. S. Wang, S. L. Huang, M. K. Lee, and C. K. Sun, "Two-photon optical-beam-induced current imaging of indium gallium nitride blue light-emitting diodes," Opt. Lett. **24**(20), 1407–1409 (1999).
12. C. J. R. Sheppard, "Aberrations in high aperture conventional and confocal imaging systems," Appl. Opt. **27**(22), 4782–4786 (1988).

13. T. Wilson and A. R. Carlini, "The effect of aberrations on the axial response of confocal imaging systems," J. Microsc. **154**(3), 243–256 (1989).
14. C. J. R. Sheppard and C. J. Cogswell, "Effects of aberrating layers and tube length on confocal imaging properties," Optik (Stuttg.) **87**(1), 34–38 (1991).
15. S. Hell, G. Reiner, C. Cremer, and E. H. K. Stelzer, "Aberrations in confocal fluorescence microscopy induced by mismatches in refractive index," J. Microsc. **169**(3), 391–405 (1993).
16. D. Ganic, X. Gan, and M. Gu, "Reduced effects of spherical aberration on penetration depth under two-photon excitation," Appl. Opt. **39**(22), 3945–3947 (2000).
17. M. J. Booth, "Adaptive optics in microscopy," Philos. Transact. A Math. Phys. Eng. Sci. **365**(1861), 2829–2843 (2007).
18. H. Jacobsen, P. Hanninen, E. Soini, and S. W. Hell, "Refractive-index-induced aberrations in two-photon confocal fluorescence microscopy," J. Microsc. **176**(3), 226–230 (1994).
19. G. Saavedra, I. Escobar, R. Martínez-Cuenca, E. Sánchez-Ortiga, and M. Martínez-Corral, "Reduction of spherical-aberration impact in microscopy by wavefront coding," Opt. Express **17**(16), 13810–13818 (2009).
20. M. Demenikov and A. R. Harvey, "A technique to remove image artefacts in optical systems with wavefront coding," Proc. SPIE **7429**, 74290N, 74290N-12 (2009).
21. J. Tang, R. N. Germain, and M. Cui, "Superpenetration optical microscopy by iterative multiphoton adaptive compensation technique," Proc. Natl. Acad. Sci. U.S.A. **109**(22), 8434–8439 (2012).
22. D.-S. Wan, M. Rajadhyaksha, and R. H. Webb, "Analysis of spherical aberration of a water immersion objective: application to specimens with refractive indices 1.33-1.40," J. Microsc. **197**(3), 274–284 (2000).
23. C. J. R. Sheppard, "Comment on 'Analysis of spherical aberration of a water immersion objective: application to specimens with refractive index 1.33-1.40', D.-S. Wan, M. Rajadhyaksha and R. H. Webb, J. Microsc. 197, 274-284 (2000)," J. Microsc. **200**(3), 177–178 (2000).
24. M. A. Neil, R. Juskaitis, M. J. Booth, T. Wilson, T. Tanaka, and S. Kawata, "Adaptive aberration correction in a two-photon microscope," J. Microsc. **200**(2), 105–108 (2000).
25. J. F. Mann, E. Shakir, K. C. Carter, A. B. Mullen, J. Alexander, and V. A. Ferro, "Lipid vesicle size of an oral influenza vaccine delivery vehicle influences the Th1/Th2 bias in the immune response and protection against infection," Vaccine **27**(27), 3643–3649 (2009).
26. F. Bestvater, E. Spiess, G. Stobrawa, M. Hacker, T. Feurer, T. Porwol, U. Berchner-Pfannschmidt, C. Wotzlaw, and H. Acker, "Two-photon fluorescence absorption and emission spectra of dyes relevant for cell imaging," J. Microsc. **208**(2), 108–115 (2002).
27. D. Débarre, E. J. Botcherby, T. Watanabe, S. Srinivas, M. J. Booth, and T. Wilson, "Image-based adaptive optics for two-photon microscopy," Opt. Lett. **34**(16), 2495–2497 (2009).
28. N. Ji, T. R. Sato, and E. Betzig, "Characterization and adaptive optical correction of aberrations during in vivo imaging in the mouse cortex," Proc. Natl. Acad. Sci. U.S.A. **109**(1), 22–27 (2012).
29. M. Rueckel, J. A. Mack-Bucher, and W. Denk, "Adaptive wavefront correction in two-photon microscopy using coherence-gated wavefront sensing," Proc. Natl. Acad. Sci. U.S.A. **103**(46), 17137–17142 (2006).
30. P. N. Marsh, D. Burns, and J. M. Girkin, "Practical implementation of adaptive optics in multiphoton microscopy," Opt. Express **11**(10), 1123–1130 (2003).

1. Introduction

The advantages of multi-photon laser scanning microscopy (MPLSM) are well established [1–4] and developments in instrumentation and photochemistry are constantly on-going in order to obtain as much information as possible from the biological specimen. Some of the most recent developments in laser instrumentation for MPLSM provide ultra-short pulsed output at wavelengths longer than the Ti:Sapphire laser, and reports of improved specimen viability and greater depth penetration into thick tissue are very encouraging [5–9].

However, the growing trend in the application of longer wavelengths (λ>850 nm) for MPLSM presents a challenge for the microscope optics, most specifically the objective lens. Usually designed for use with visible light, standard objective lenses have good chromatic correction in the λ = 400–700 nm region but perform less well at longer wavelengths [10]. Recently, objective lenses specifically for MPLSM have been introduced by a few manufacturers. These have higher transmission at long wavelengths but this is now rarely necessary as most ultra-short pulsed lasers provide more average output power than is required for imaging.

Spherical aberration seems to be a more serious problem, which causes four difficulties in imaging. Firstly, a loss of axial resolution is incurred, which can result in blurring [11]. The consequences of aberrations upon axial resolution have been considered previously [12,13]. Within these analyses the effect of the aberration is described by the arbitrary function ϕ. This function was later defined by Sheppard and Cogswell [14] in terms of a beam focusing into a specimen of refractive index n_2, which is mounted in a medium of refractive index n_1

$$\varphi = tk(n_2 - n_1)\left[1 + \frac{2n_1}{n_2}s^2 + 2(n_2 + n_1)\frac{n_1^2}{n_2^3}s^4 + ...\right] \qquad (1)$$

where t is the thickness of the layer, k is the wavenumber ($k = 2\pi/\lambda$), $s = \sin(\theta_1/2)$ with θ_1 equal to the angle of incidence of a ray within the light cone, and the term containing s^4 representing the contribution of the primary spherical aberration. From Eq. (1) it is clear that spherical aberration is wavelength dependent, and that the effect is reduced at long wavelengths.

Secondly, substantial shifts in the focal plane may result, which are particularly inconvenient for applications such as genome organization, whereby defocusing shifts on the micrometer scale can lead to incorrect identification of chromophore locations [15]. This defocus is described by the term containing s^2 in Eq. (1).

Thirdly, depth penetration is severely reduced when spherical aberration is acute. Deep tissue imaging is central to the rapidly expanding field of *in vivo* imaging of intact specimens and live animals that allows researchers to observe biological processes without the need for invasive sectioning techniques [2]. It is reported experimentally that MPLSM experiences less spherical aberration than single-photon imaging at equivalent depths [16], however as the depth penetration of MPLSM is often substantially greater than for single photon techniques, compensation of spherical aberration becomes increasingly important in order to resolve the maximum possible detail from the specimen. Finally and, in the case of biological imaging, most importantly, the loss of signal incurred through spherical aberration can lead to the researcher applying damaging levels of irradiation at the specimen in attempting to acquire an image [17]. A full experimental and theoretical description of the drop in fluorescence incurred whilst performing MPLSM at depth has been previously presented by Jacobsen *et al.* [18].

One technique used to compensate for spherical aberration is the use of a correction collar on the objective lens. This method involves translating a lens or group of lenses within the barrel of the objective to introduce an aberration opposite in sign to that which needs correction. However, this form of correction is limited to imaging close to the surface of a specimen. An excellent review of this technique is given by Sheppard and Gu [7]. Despite the usefulness of this approach, however, no commercial water dipping lenses have a correction collar. Thus in cases where a water dipping lens is required and the refractive index mismatch is large, spherical aberrations cannot be corrected.

Adaptive optical devices provide an active means of compensating for spherical aberration. In a similar fashion to a correction collar, these devices pre-aberrate the wavefront by imposing the opposite value of aberration to that induced by the specimen. For a thorough review of these devices see Booth [17]. Despite the very good results produced by this method, the high cost for deformable mirrors and spatial light modulators and the need for complex algorithms that are often coupled with long pre-imaging exposure to optimise the mirror configuration limit the effectiveness of this technique for tissue MPLSM.

A further technique which can be used to reduce the impact of spherical aberration and increase the imaging depth of field is wavefront coding. This method combines the use of a phase mask along with a digital image restoration process [19]. Together, these can be used to provide improved collection of data from deep within a specimen. However, inherent noise artifacts limit the potential of this technique. Moreover, additional complex and iterative manipulation of the phase mask is required [20], resulting in long exposure times which makes it unsuitable for application to biological specimens.

Recently an exciting development in MPLSM aberration correction technology has been presented. This is known as the iterative multi-photon adaptive compensation technique (IMPACT) and is a system which takes advantage of the nonlinearity of the multi-photon process to determine, and compensate for, distortions and aberrations incurred throughout a specimen [21]. This technique has been shown to provide diffraction limited imaging at depths beyond the possibilities of conventional MPLSM. This depth improvement is coupled

with greatly improved signal strength of up to two orders of magnitude. In addition to these impressive benefits, acquisition speeds are improved by ten-fold over standard adaptive optics techniques. However, one limitation of IMPACT is that the improvement of the imaging is only in the central section of the excitation beam. This means that the field of view in each image is small and laborious stitching of images is required.

We present here a simple technique whereby spherical aberration can be greatly reduced for long wavelengths ($\lambda > 850$ nm) used in MPLSM simply by changing the immersion medium. A similar technique to this has been previously demonstrated by Wan *et al.* [22], where the immersion liquid was tailored to suit the specimen, resulting in reduced spherical aberration. However, no details of the alternative liquids were given, solely a list of refractive indices, making it difficult to reproduce these results [23].

Our method, which is compatible with standard MPLSM systems, consists simply of using methanol immersion (MI) as an alternative to water immersion (WI). Correction of the spherical aberration of the axial point spread function of the fluorescence image and up to a 6-fold increase in the fluorescence signal intensity was observed and there was a more than 2-fold increase in depth penetration. The approach was compatible with standard methods of specimen preparation for epi-fluorescence, including immunofluorescence and did not alter the morphology of fixed tissues.

2. Experimental set-up

Experiments were performed using three microscope systems and three different water dipping objective lenses. The first was an ultra-short pulsed Ti:Sapphire (Chameleon, Coherent Inc.) coupled to a commercial laser scanning microscope (Leica TCS SP5 and DM6000 upright microscope, used with the water dipping lens HCX APO L 40x/0.80 N.A. W with a working distance of 3.3 mm). The second system was an ultra-short pulsed Ti:Sapphire (Mira 900-F, Coherent) coupled to a commercial laser scanning microscope (Olympus FV300 and IX71 microscope, used with an Olympus water dipping lens LUMPlanFN 60×W, 60×/1.0 N.A, with a working distance of 2.0 mm). The third system was an Yb:fibre laser (HP-1060-2, Fianium) coupled to a home-built laser scanning microscope used with a NikonCFI Fluor 60×W 60×/1.0 water dipping lens with a working distance of 2.0 mm. For all three platforms similar results were achieved: for clarity, only the data from the Leica SP5 microscope are presented here.

The excitation source used was a wavelength tunable Ti:Sapphire laser (Chameleon VISION II, Coherent Inc.) with $\lambda = 680$–1080 nm, repetition rate of 76 MHz and pulse durations of ~140 fs across the full wavelength tuning range. In order to implement methanol as an immersion medium, an immersion well surrounding the specimen was required (as shown in Fig. 1). This was required because methanol has a lower surface tension than dH$_2$O (22.70 mN/m for methanol, compared with 72.80 mN/m for dH$_2$O) and so a well was necessary to bridge the large gap between the objective and the top of the specimen. In this experiment the well consisted of a 3 mm thick aluminium plate cemented to the glass microscope slide, with a 13 mm hole surrounding the specimen. Commercial well slides (Ibidi) were also found to be suitable, depending on the specimen to be imaged.
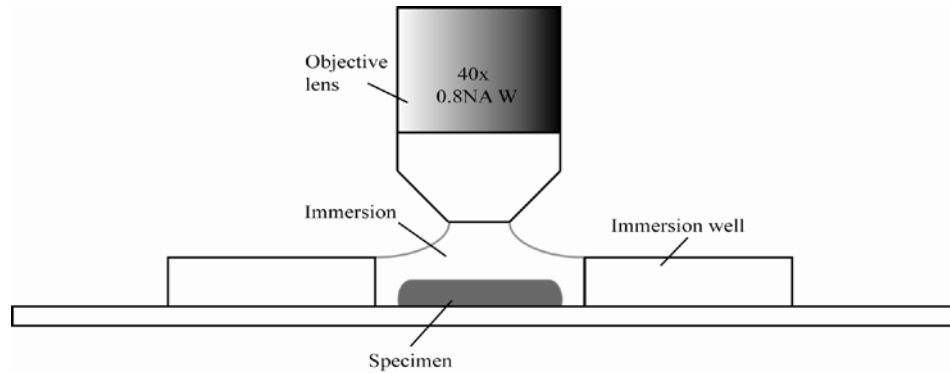
Fig. 1. Immersion well tailored to a water dipping lens for use with methanol immersion (MI).

Using a spectrometer (Lambda 12, Perkin Elmer), the linear absorptions for both water and methanol were measured over the wavelength range used in this experiment, λ = 700–1050 nm, at 50 nm intervals (data not shown). This allowed us to ensure that absorption differences between WI and MI were compensated for by changing the peak power accordingly. Equivalent levels of irradiation were provided at the specimen in both cases. Three different specimens were imaged using WI and MI.

To determine if spherical aberration was present over the range of wavelengths when applying both WI and MI, we adopted a similar approach to Neil *et al.* [24] and performed XZ sectional imaging of a reference slide of fluorescent beads (6 μm diameter Fluoresbrite, Polysciences Inc.) attached to a microscope slide by allowing the water in which they were suspended to evaporate. Here, line intensity plots through the centre of each bead were collected over a wavelength range of λ = 700–1050 nm, in 50 nm steps, in order to visualise the degree of symmetry in the axial intensity distribution, with increased asymmetry indicating increased spherical aberration.

Images were taken at a frame rate of 2 Hz, 5× digital zoom with a box size of 512 × 512 pixels. The average power delivered to the specimen plane for imaging was kept constant for each different wavelength at 8 mW. The pulse duration reaching the specimen in the case for WI and MI was considered to be the same. This assumption was based upon no change in pulse duration measured from autocorrelation measurements taken before and after pulse propagation from λ = 700–1050 nm through both 3 mm of water and then methanol within a cuvette (data not shown).

Using imaging software (ImageJ, NIH), line intensity profiles could be extracted through the centre of the bead. This was carried out for five beads (n = 5) at each wavelength and averages were recorded. In the absence of spherical aberration, symmetrical Gaussian intensity profiles were to be expected [11]. Using MATLAB (Mathworks), a theoretical least squares Gaussian fit was applied to the data, from which the error from the fit served as an indicator of the level of spherical aberration. In this experiment, the detector gain was adjusted to give similar fluorescence signal levels from all images, and linescan intensity data was normalised before fitting to the Gaussian in order to facilitate direct comparison of the WI and MI cases. For all other experiments thereafter, the detector gain level was kept constant at all excitation wavelengths and for both WI and MI.

Following data acquisition to investigate the degree of spherical aberration across the λ = 700–1050 nm wavelength range for both WI and MI and again using ImageJ, fluorescence intensity levels were measured for n = 5 beads for both WI and MI across the same wavelength range.

After the initial experiments with fluorescent beads to determine the level of spherical aberration observed using excitation wavelengths from λ = 700–1050 nm for both WI and MI, we imaged two different thick and fluorescently labeled biological specimens. The first specimen was a 2 mm thick section of mouse brain labeled with fluorescein isothiocyanate (FITC) secondary antibody recognising primary antibodies against alpha-tubulin cytokeletal

protein. Tissue had been fixed with 4% (v/v) paraformaldehyde, permeabilised with PBS/TWEEN and blocked with 0.2% (v/v) donkey serum prior to antibody incubations. The second specimen was a 1 mm thick section of rat intestine labeled with Texas Red. Rats (adult male, Sprague Dawley) were starved for two hours prior to administration with 200µl of Bilosomes loaded with OVA-Texas Red [25]. Sections (2cm) of intestine with visibly identified areas of Peyer's Patches were collected and washed several times with phosphate buffered saline, pH7.4 and then 1 mm thick sections were fixed on glass slides using one drop of tissue adhesive (Vetbond, 3M). The excitation wavelengths used for brain and gut imaging were 950 and 1000 nm respectively. These values were chosen based upon the wavelengths that provided the highest two photon response. Filter-free beam splitting spectral detection was applied to provide detection range from $\lambda = 500$–600 nm for the brain and $\lambda = 530$–630 nm for the gut. Imaging acquisition in both specimens were kept constant (frame rate of 2 Hz, a box size of 512×512 pixels, with n = 8 Kalman average scan). As above, ImageJ was used to compare detected fluorescence signal intensities under WI and MI for the brain section. A comparison of depth imaging within the gut section was then carried out for both WI and MI, using ImageJ to measure the depth of penetration at a fixed wavelength of 1000 nm, where refractive index mismatch was found to be high.

3. Results

3.1 Spherical aberration: XZ linescans comparing WI and MI

Figure 2 shows images of 6 µm diameter beads using excitation at two different wavelengths, $\lambda = 750$ nm and $\lambda = 1000$ nm, under WI and MI. By measuring the axial intensity profile through the bead (a) and (b) it was confirmed that methanol and water immersion of the specimen generate similar Gaussian intensity profiles when imaging at $\lambda = 750$ nm. However, as is shown in (c) and (d), when exciting at a wavelength of $\lambda = 1000$ nm, MI provided a distribution close to Gaussian, unlike WI, which produced a skewed Gaussian that is indicative of spherical aberration. In Fig. 2 we note that the detector gain has been altered for each image in order to have comparable images for illustration purposes (differences in fluorescence intensity when using MI compared with WI are described in detail in the next section).
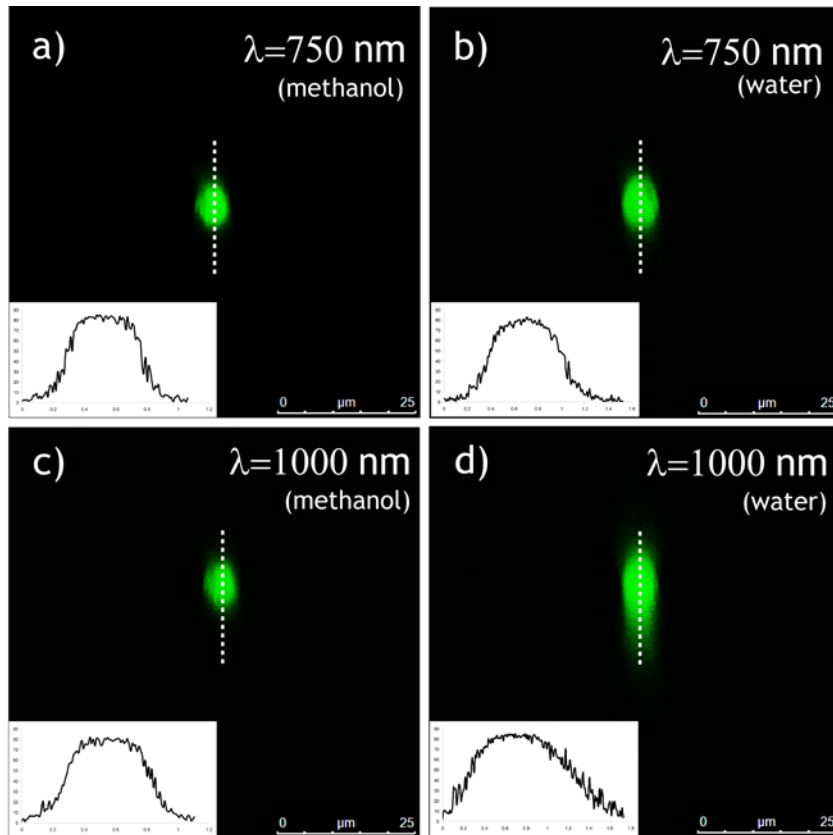
Fig. 2. XZ MPLSM images and inset linescans through the centre of a 6 μm diameter fluorescent bead imaged with an excitation wavelength of λ = 750 nm for (a) MI and (b) WI, and imaged with an excitation wavelength of λ = 1000 nm for (c) MI and (d) WI, accompanied by the line intensity plots at the centre of the bead. The detector gain was adjusted in order to provide illustrative examples. For all data following this figure, the detector gain was kept constant during imaging with WI and MI.

Applying a least-squares Gaussian fit to the intensity linescans of n = 5 beads imaged with excitation wavelengths of λ = 700–1050 nm in 50 nm increments, the errors from the fit for both WI and MI are presented in Fig. 3. Across the excitation wavelength range λ = 700–850 nm, the error is between 10 and 12% for both WI and MI, indicating a similar level of spherical aberration for both immersion media. However, when increasing the wavelength beyond λ = 850 nm, an increase in the error from the Gaussian fit was observed with WI, indicating progressively increased spherical aberration at longer wavelengths. In contrast to this, with MI the error from Gaussian fit decreases with wavelength, indicating progressively decreased spherical aberration at longer wavelengths.
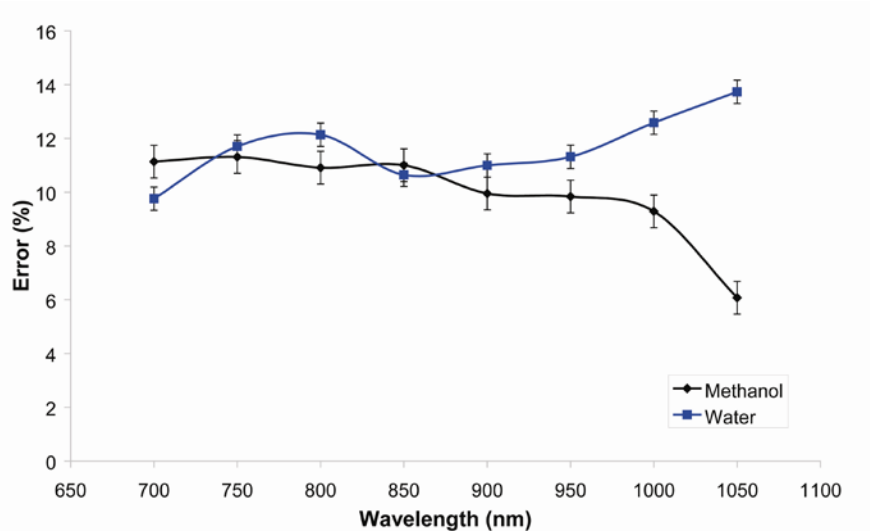
Fig. 3. Average error from the Gaussian fit to the intensity line scans of 6 μm diameter fluorescent beads as a function of excitation wavelength. These data are accompanied by the standard error for each data point (n = 5 beads at each wavelength).

3.2 Fluorescence signal intensity measurements: comparing WI and MI

Whilst imaging the fluorescent polystyrene beads with both WI and MI in section 3.1, it was found that a fluorescence increase in excess of ten-fold was observed at the longer wavelengths of the Ti:Sapphire when applying MI (data not shown).

   To illustrate the usefulness of aberration correction at long wavelengths within biological specimens, a comprehensive comparison between WI and MI was carried out for two thick sections of rodent tissue. Figure 4(a) shows the measured fluorescence signal intensity when applying WI or MI to the same region, at a depth of 100 μm, within a thick brain slice labeled with FITC. The data correlate well with the spherical aberration highlighted in Fig. 3, where little difference in fluorescent signal intensity was observed when spherical aberrations are similar i.e. at $\lambda < 900$ nm. Yet as spherical aberration increases, i.e. at $\lambda > 900$ nm, the ratio of MI/WI florescence signal intensity increased. It was noted that despite the fluorescence intensity dropping substantially at wavelengths above $\lambda = 950$ nm (as expected because of the reduced two-photon excitation cross-section of FITC at longer wavelengths [26]) the ratio of MI/WI fluorescence signal intensity remained high. Figures 4(b) and 4(c) show example XY cross-sectional MPLSM images of the brain slice obtained with an excitation wavelength of $\lambda = 950$ nm (where the highest fluorescence signal intensity increase was observed) for MI and WI respectively.
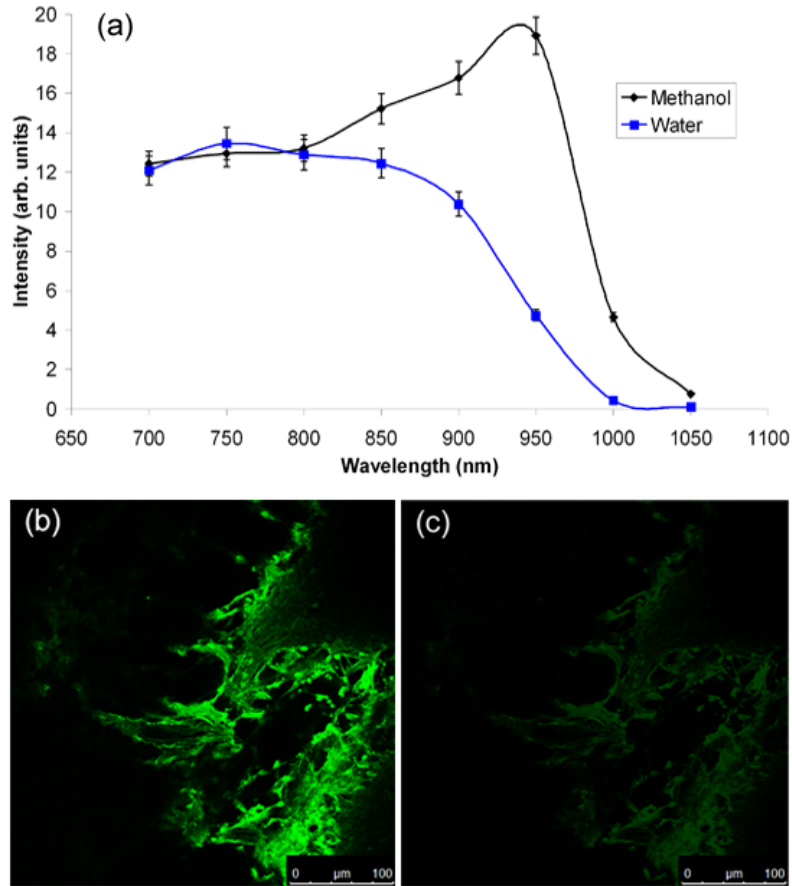
Fig. 4. Brain section. (a) Measured average fluorescence signal intensity of the entire images as a function of wavelength for WI and MI. These data are accompanied by the standard error for each data point (n = 5 images at each wavelength). Note that the low dynamic range of the graph is solely due to the averaging of the entire image. XY images of brain section with (b) MI and (c) WI using the same gain level, excitation wavelength of λ = 950 nm, average power of 20 mW at the specimen plane, 2 Hz capture rate, a box size of 512 × 512 pixels and n = 8 Kalman averaging.

3.3 Depth penetration

To determine the effect of MI spherical aberration correction upon depth penetration, the 1 mm thick specimen of rat gut was imaged with both WI and MI. At a fixed depth of 100 μm, similar increases in fluorescence intensity were observed as to that found in the brain section shown in Section 3.2. The gut section was selected for this analysis as it exhibited fluorescence deep below the surface of the tissue.
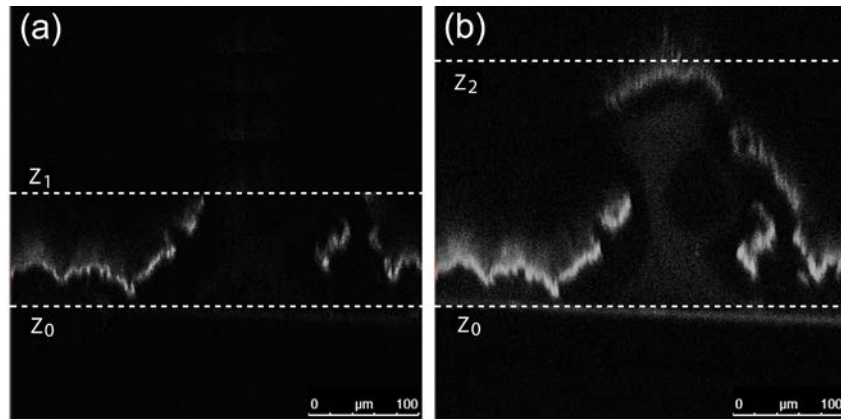
Fig. 5. Gut section - XZ scan showing depth penetration attainable with (a) WI and (b) MI. More than a two-fold increase in depth was observed when using MI at the same excitation and image capture parameters. (λ = 1000 nm, 20 mW, 2 fps, 512 × 512 pixels, n = 8 Kalman averages).

Figures 5(a) and 5(b) show XZ scans for a section of gut using WI and MI respectively at an excitation wavelength of λ = 1000 nm and detection range of λ = 530–630 nm. The images are shown in Grayscale in order to provide high contrast for ease of viewing. The dashed line at Z_0 on each image represents the surface of the specimen. In image (a), Z_1 corresponds to the imaging depth at which the signal falls to zero for WI, which equates to a distance of 110 µm from Z_0 to Z_1, whilst Z_2 corresponds to double the depth of Z_1. It is noted that low levels of fluorescence are also found beyond the depth of Z_2.

4. Discussion

By reducing spherical aberration at excitation wavelengths longer than λ = 850 nm, more than a six-fold increase in fluorescence signal intensity and in excess of a two-fold increase in depth penetration were obtained when using MI rather than the conventional WI with water dipping lenses.

The six-fold fluorescence signal increase using MI compared to WI improves on previously reported adaptive optical methods of spherical aberration correction within biological tissue: Debarre *et al.* reported only a two-fold increase in fluorescence signal intensity using adaptive optics when imaging a mouse gut similar to the specimen used in this paper [27] although, enhancements of up to five-fold have also been observed within mouse brain [28]. As discussed previously, a ten-fold increase in fluorescence was also observed in our reference slide of fluorescent beads. This compared well to the observation of a six-fold increase in fluorescence when comparing to adaptive wavefront correction for imaging of polystyrene beads [29]. Our MI method performs less well than common adaptive optical methods at depth: our two-fold increase in depth penetration does not match previously reported order-of-magnitude results [30]. However, we note that their result was achieved in a non-biological specimen where the refractive index mismatch was designed to be high and also that our passive method yields an instantaneous result, with no optimization of optoelectronic components required. This minimizes the radiation dose to the specimen and also reduces the time taken for each experiment, which in turn is likely to reduce photo-damage to the specimen. Nevertheless, rather than replacing adaptive optical methods, we see MI as a complementary method that may reduce the degree of spherical aberration correction required of active elements.

We note that the increase in fluorescence intensity observed when using MI in comparison with WI does not seem to be related to electronic or chemical change in the fluorophore when immersed in methanol. Experiments were performed with fixed specimens mounted under a coverslip with dH_2O or methanol between the coverslip and the lens so that no interaction between the fluorophore and the immersion material could occur. The results from this were

similar to those obtained when imaging without a coverslip; at shorter wavelengths, the fluorescence intensity observed was similar for both WI and MI, whereas a four-fold increase in fluorescence signal intensity was measured at long wavelengths when using methanol rather than dH_2O. Although this fluorescence increase at long wavelengths was less than the six-fold increase observed when imaging with no coverslip, we attribute this to the additional spherical aberration incurred by the introduction of the coverslip.

Although methanol is sometimes used as a fixative and has a strong dehydration effect, imaging was possible with no obvious change in structure to any of the specimens over a two hour MPLSM imaging period with continuous immersion in this solvent.

Since methanol is miscible in water, it may prove useful to vary the proportions of water and methanol (or other liquids) to create a full spectrum of immersion liquids that could be matched to different types of tissue for better index matching. Although not investigated here, the use of alternative immersion materials with oil immersion objective lenses may also provide similar or better spherical aberration correction at long wavelengths. Also, we used an ultra-short pulsed Ti:Sapphire laser for this investigation: the improvement at yet longer wavelengths provided by alternative sources may be even greater.

The striking improvements in sensitivity and depth of imaging revealed as possible by our simple method with fixed specimens may perhaps stimulate the manufacturers to develop spherical aberration correction for dipping objectives by the more convenient method of turning a correction collar, which may well improve performance with water and living material.

5. Conclusion

Application of methanol as an immersion liquid to dH_2O has been described. With more than a six-fold increase in fluorescence signal intensity in biological tissue, and penetration depth into thick tissue increased by more than a factor of two, this adaptation could have widespread use in biological imaging. Although our study was limited to methanol as an immersion fluid, other alternative immersion liquids may provide yet further correction at $\lambda > 850$ nm wavelengths used in MPLSM.

Acknowledgment